ACS ES&T Engineering

pubs.acs.org/estengg

Article

Bicarbonate-Carbonate Selectivity through Nanofiltration for Direct Air Capture of Carbon Dioxide

Anatoly Rinberg* and Michael J. Aziz

Cite This: https://doi.org/10.1021/acsestengg.4c00150

Read Online

ACCESS | Metrics & More | Article Recommendations | Supporting Information

ABSTRACT: Direct air capture (DAC) of carbon dioxide is one approach among many proposed that is capable of offsetting hard-to-avoid emissions. In previous work, we developed the alkalinity concentration swing (ACS) method, which is driven through concentrating an alkaline solution that has been loaded with atmospheric CO_2 by desalination technologies, such as reverse osmosis or capacitive deionization. Though the ACS is promising in terms of energy usage and implementation, its absorption rate and water requirements are infeasible for a large-scale DAC process. Here, we propose an improvement on the ACS, the bicarbonate-enriched alkalinity concentration swing (BE-ACS), which selects bicarbonate ions from a stream of aqueous alkaline solution that has absorbed atmospheric CO_2. The bicarbonate-rich stream is then concentrated, which greatly increases its CO_2 partial pressure, and then CO_2 is extracted from solution. We experimentally investigate the use of pressure-driven nanofiltration (NF) membrane-based separation to select bicarbonate ions over carbonate ions. We screen commercial membranes and select one high-performance membrane for detailed studies, quantifying its bicarbonate-carbonate selectivity factor and bicarbonate-passage factor. Feed pH, the combined concentration of aqueous CO_2, bicarbonate, and carbonate species (or dissolved inorganic carbon), alkalinity, and permeation flux are systematically varied to study NF separation properties. We find that the selectivity factor, which exceeds 30 times in certain regimes, increases with higher feed pH and higher alkalinity. The performance metrics of the selected NF membrane are input into a theoretical BE-ACS cycle analysis, and the required energy input and cycle capacity output are evaluated. Ideal cycle energy is found to be as low as around 250 kJ/mol, with opportunities identified for further decreases through process engineering and forward osmosis energy recovery.

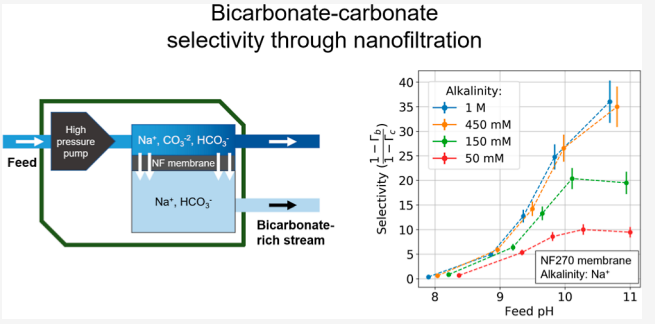

KEYWORDS: *carbon dioxide removal, direct air capture, carbon dioxide, dissolved inorganic carbon, nanofiltration*

1. INTRODUCTION

Climate change, driven by an increasing rate of anthropogenic greenhouse gas emissions, has resulted in a pressing need to globally manage carbon sources and sinks. Reducing emissions as much and as rapidly as possible must be prioritized to avoid the worst harm from global warming, which will be felt most by vulnerable populations. In addition to emission reductions, in its Sixth Assessment Report, the Intergovernmental Panel on Climate Change states that the "deployment of carbon dioxide removal (CDR) to counterbalance hard-to-abate residual emissions is unavoidable if net zero CO_2 or [greenhouse gas] emissions are to be achieved."[1] In other words, it is now the case that, if global warming is to be halted this century, gigaton scale of annual CDR will be needed to offset hard-to-avoid emissions,[2] especially those from agriculture and long-haul aviation. However, aiming for 10 to 20 billion tons of removal by mid to late century, as many reports and policy proposals are advocating,[3] brings along significant moral hazard, as it reduces the political incentive to pursue the challenging task of decarbonizing society today.[4,5]

1.1. Direct Air Capture.

CDR approaches span a broad range, from land and ocean-based methods, such as reforestation, shifts in agricultural practices, and the addition of alkalinity into the ocean, to industrial methods, such as enhanced mineralization and direct air capture (DAC) with carbon storage (DACCS).[6,7] DACCS, in particular, is a highly energy-intensive physicochemical process for capturing atmospheric CO_2, concentrating and compressing it, and then durably storing it in geological reservoirs or materials. Although exceptions exist, DAC methods are broadly split into two categories: one that is based on reversible adsorption onto a solid sorbent and another that is based on reversible dissolution into a solvent. Each approach confers its own

Received: March 21, 2024
Revised: May 27, 2024
Accepted: May 28, 2024

advantages. Solid sorbents, which often rely on amine polymers to react with CO_2, require only low-grade heat or moisture for regeneration but rely on minimal water usage.[8] Solvent-based approaches often require large amounts of water or other solvents, but they have the advantage of decoupling contacting from regeneration, allowing for continuous absorption.[9,10]

This work builds on the body of research of aqueous solvent DAC approaches, which has recently been focused on electrochemical methods.[11−15] Electrochemical DAC has the advantage of feasibly reaching low energy of capture, below 100 kJ/mol; however, the various approaches still face implementation challenges relating to chemical degradation, membrane stability and fouling, low kinetics of reaction, and more.[16]

We report the first experimental demonstration of a bicarbonate-carbonate selectivity step used for DAC through an osmotic pressure drive, specifically nanofiltration (NF) membrane-based separation. These desalination technologies have been widely deployed on an industrial-scale for decades and benefit from extensive material and process engineering, resulting in energy efficiency and material stability.[17,18] Previously, reverse osmosis (RO) and capacitive deionization methods were proposed as drivers of a concentration-based process, the alkalinity concentration swing (ACS).[19−21] These desalination approaches were shown to be effective at concentrating dissolved inorganic carbon (DIC)—aqueous CO_2, bicarbonate, and carbonate species. However, challenges relating to the operation of desalination technologies at high CO_2 partial pressure, as well as rate and water limitations of the ACS cycle, were identified as improvement targets to attain feasible large-scale deployment.[22] In this work, demonstrating the selection of bicarbonate ions using NF in a solution of DIC represents experimental evidence for significantly improving the ACS. Beyond DAC, this work is broadly relevant to methods that rely on controlling alkalinity and DIC concentrations and their ratio, such as electrodialysis or electroreduction.[23,24]

1.2. Enhancing the ACS with Bicarbonate-Carbonate Selectivity. The bicarbonate-enriched alkalinity concentration swing (BE-ACS) is a proposed process for enhancing ACS through bicarbonate-carbonate selectivity. Without modification, the ACS absorption rate and water requirements were identified as being impractical for large-scale implementation. Whereas the ACS simply concentrates feed solution to increase its CO_2 partial pressure, the BE-ACS first splits the feed into bicarbonate-rich and carbonate-rich streams. The bicarbonate-rich stream is then concentrated, resulting in a higher solution CO_2 partial pressure and therefore higher cycle capacity than is otherwise possible. Outgassing from the concentrated bicarbonate-rich solution results in the following disproportionation reaction

$$2HCO_3^- \rightarrow CO_2(aq) + CO_3^{-2} + H_2O \quad (1)$$

Once CO_2 is collected from the concentrated bicarbonate-rich stream, it is recombined with the diluted stream and the carbonate-rich stream and sent for CO_2 absorption. The selectivity step and the higher cycle capacity also mean that the BE-ACS further confers advantages on the absorption rate.

1.3. Ion Selectivity through NF. RO and NF are both membrane-based pressure-drive separation methods, which block solutes in solution from passing. Unlike RO membranes, which have pore sizes of less than 1 nm and tend to block monovalent and divalent ions with >99% effectiveness,[18,25] NF membranes operate with larger pore size from 1 to 10 nm, making them well-suited for separating monovalent and divalent ions. The particular pore size window, along with the fixed membrane charge, makes NF an effective technology for water softening, lithium/magnesium separation, chloride-sulfate separation, and generally acid−base separation.[26−30] Up until this work, bicarbonate-carbonate separation with NF membranes has not been systematically evaluated.

The underlying mechanisms for this separation are based on multiple effects, including steric partitioning, diffusion, and advection; however, two contribute most dominantly: Donnan potential and electromigration.[31] The first is the result of an entropic force that is generated by a high internal membrane charge concentration. The inability of the membrane-charged groups to equilibrate with the solution establishes a potential field, called the Donnan potential, and applies a force on the feed ions that differs depending on their valence charge. The second is electromigration, which is driven by electric fields that are established by differences in concentrations across the membrane and also acts on different ions differently due to differing valence charges. Because the drag of bicarbonate and carbonate ions in solution is very similar, a bicarbonate ion in an electric field feels roughly half of the force of a carbonate ion.

In this work, we experimentally investigate the use of NF membrane separation as a method to select bicarbonate ions and reject carbonate ions by implementing the BE-ACS selection step. We demonstrate that NF can exploit the charge difference between bicarbonate (monovalent) and carbonate (divalent) ions to create two solution streams: one bicarbonate-rich and one carbonate-rich. We combine an aqueous DIC model, the experimental NF results, and an ideal NF-RO energy model to assess two figures of merit for the BE-ACS: volumetric cycle capacity of CO_2 capture (hereafter called "cycle capacity" for brevity) and ideal cycle energy. In this work, we do not consider the average absorption flux, which is the third key figure of merit that we analyzed in past studies.

2. THEORY AND PROCESS

2.1. Equilibrium Carbonate Chemistry. The state of DIC in solution is a function of the following chemical reactions and charge-neutrality condition

$$CO_2(gas) \overset{H^{cp}}{\longleftrightarrow} CO_2(aq) \quad (2)$$

$$CO_2(aq) + H_2O \overset{K_1}{\leftrightarrow} H^+ + HCO_3^- \overset{K_2}{\leftrightarrow} 2H^+ + CO_3^{-2} \quad (3)$$

$$A = [Na^+] = [HCO_3^-] + [CO_3^{-2}] + [OH^-] - [H^+] \quad (4)$$

Here, A represents the alkalinity, defined as the molar charge difference between the sum of the conservative cations and anions, which are ions whose concentrations do not vary with pH. In this work, we assume alkalinity is equivalent to Na^+ concentration.

To study the relationship between DIC, alkalinity, and partial pressure, we developed an aqueous dissolved inorganic carbon model (ADICM), which implements the Pitzer equations through PHREEQC, as described in Section 3.4.

2.2. BE-ACS Cycle: Driven through Osmotic Pressure. Building on our previous work, which comprehensively

https://doi.org/10.1021/acsestengg.4c00150
ACS EST Engg. XXXX, XXX, XXX−XXX

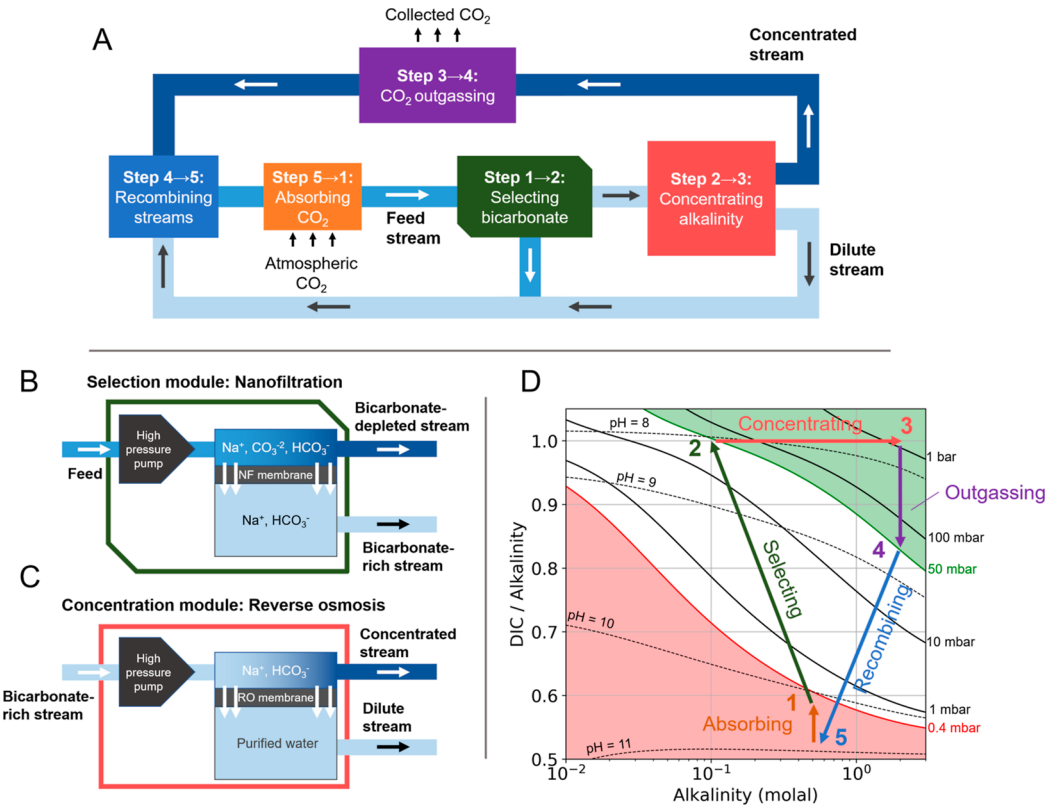

Figure 1. NF and RO for the BE-ACS. (A) Five steps of the BE-ACS represented through a flow diagram. (B) Schematic of the NF selection module, depicting a feed being pressurized by a pump and a bicarbonate-rich solution being permeated through the membrane. (C) Schematic of a RO concentration module. The bicarbonate-rich stream is passed into the RO module, producing a concentrated stream, which is sent for CO_2 outgassing, and a dilute stream. (D) DIC-to-alkalinity diagram and the five steps of the BE-ACS. Dashed lines correspond to iso-pH curves in the diagram; solid black lines correspond to iso-pCO_2 points. The red line corresponds to 0.4 mbar (or 400 ppm), which sets the maximum feed starting point for atmospheric capture. The green line is a 50 mbar threshold, chosen arbitrarily as an outgassing target that is above the vapor pressure of water.

characterized BE-ACS theoretically, this section focuses on the two steps that can be implemented through osmotic pressure: the selection and concentration steps of the cycle. As depicted in Figure 1, in step 1 → 2, feed solution is passed through a bicarbonate-carbonate selection module. In this work, we investigate using NF membrane separation for the selection module (Figure 1B). The bicarbonate-enriched solution is then passed through a concentration module, thereby removing dilute water (step 2 → 3). We assumed an ideal RO process for this step (Figure 1C). The concentrated stream of alkalinity and bicarbonate ions is then exposed to an outgassing module to collect CO_2 (step 3 → 4). The outgassed solution with depleted DIC is then rediluted (step 4 → 5) and sent to an ambient air contactor for CO_2 absorption (step 5 → 1).

2.2.1. Step 1 → 2: Selecting Bicarbonate Using NF. The feed condition of the solution is set by the initial alkalinity (A_1) and initial DIC ($C_{DIC,1}$) concentrations (state 1), which corresponds to a feed solution CO_2 partial pressure, p_{in}. Note that p_{in} is a property of the solution rather than of the gas to which it is exposed. For ease of notation, we introduce the following convention: $[HCO_3-] = b$ and $[CO_3^{-2}] = c$, allowing us to write the feed bicarbonate and carbonate concentrations as b_1 and c_1, respectively.

The DIC-to-alkalinity ratio is a key cycle parameter that also characterizes the fraction of bicarbonate or carbonate ions in solution. C_{DIC}/A approaching 1 is around neutral pH, bicarbonate-rich condition; C_{DIC}/A approaching 0.5 is a high pH, carbonate-rich condition. This metric is particularly useful for the ACS process because increasing alkalinity while holding the DIC-to-alkalinity constant corresponds to an ideal concentration process (Figure 1D).

In a NF process, osmotic pressure applied to a feed solution drives water and species separation, creating a permeate stream and a concentrate stream. Each species i has a corresponding rejection coefficient, Γ_i, which corresponds to the fraction of ions of a given species relative to the feed that is effectively blocked by the membrane and does not pass into the permeate. This is described in detail in Section 3.2.

Two material properties relevant for assessing BE-ACS performance quantify how bicarbonate and carbonate ion concentrations change as they pass through a NF membrane. First, we define the bicarbonate-carbonate selectivity factor in terms of rejection coefficients

$$S_{b,c} = \frac{1 - \Gamma_b}{1 - \Gamma_c} \tag{5}$$

Second, the effective bicarbonate passage fraction

$$P_b = 1 - \Gamma_b \tag{6}$$

This factor is considered "effective" because of the nonconservative nature of the DIC system: aqueous CO_2, bicarbonate, and carbonate ions can react to interconvert. Therefore, it is impossible to directly differentiate between a bicarbonate ion physically passing through the membrane and,

https://doi.org/10.1021/acsestengg.4c00150
ACS EST Engg. XXXX, XXX, XXX−XXX

Table 1. NF Membrane Characterization

membrane specifications			experimental characterization[a]			
membrane	pore size (Da)	polymer	selectivity ($S_{b,c}$)	bicarbonate passage (P_b, %)	permeate flux (LMH)	selection criterion ($S_{b,c}$*P_b)
suez DL	150−300	polyamide-TFC	28	20	168	5.6
filmtec XC-N		polypiperazine	28	22	179	6.1
snyder NFX	150−300	polyamide-TFC	19	8.0	79.5	1.5
trisep TS80	150	polyamide-TFC	18	37	237	6.5
filmtec NF270	300−400	polypiperazine	14	61	268	8.7
suez DK	150−300	polyamide-TFC	11	16	141	1.8
trisep XN45	500	polypiperazine-amide	10	60	295	5.9
snyder NFW	300−500	polyamide-TFC	8.3	61	208	5.1
trisep SB90	150	cellulose Acetate	4.8	13	27.3	0.6
suez duracid NF	150−200	polyamide-TFC	2.9	30	91.8	0.9
microdyn NP030	500	PES	1.3	93	192	1.2

[a]Characterization reported at 150 mM Na^+ and 62.5% DIC feed solution conditions. Membrane specifications are reported based on manufacturer's information. Based on measurement and instrument uncertainty, measured values are expected to have a 10% error margin. Flux is measured in units of liters per square meter of membrane per hour (LMH).

for example, a carbonate ion passing and reacting with a proton. Nevertheless the effective bicarbonate passage fraction is a key metric to characterize the effectiveness of membranes to enrich bicarbonate ions and reduce carbonate ion concentrations in the permeate.

Whereas the ideal regime for the selectivity-enhanced ACS would appear to simultaneously allow all bicarbonates to permeate ($P_b = 1$) and block all carbonates ($\Gamma_c = 1$), higher performance is possible in principle. In the case of negative rejection coefficients, as has been demonstrated in certain NF conditions,[32] bicarbonate concentration can be higher in the permeate than the feed, making $P_b > 1$ possible.

Once the feed is processed through the selection module, the post-selection solution (state 2) is characterized by its alkalinity (A_2), as well as its bicarbonate (b_2) and carbonate (c_2) concentrations. A volume fraction parameter, ϕ_s, must also be introduced to represent the fraction (0−1) of the feed solution that is output through the NF module as a bicarbonate-rich stream.

2.2.2. Step 2 → 3: Concentrating Alkalinity Using RO. The bicarbonate-rich permeate from the NF module is passed into the input stream of the RO concentration module. RO processes are characterized by high rejection coefficients for all ions, creating a highly dilute and concentrated stream. In this work, we assume an ideal RO step, with $\Gamma_{i,RO} = 1$ for all species. This assumption has an important shortcoming because, even though >99.9% rejection can be reached for sodium ions through commercial RO processes,[33] dissolved gases are not blocked by RO membranes. In practice, the loss of CO_2 through the RO membrane can be overcome by extracting CO_2 from the dilute stream in addition to the concentrated stream.

In the post-concentration solution (state 3), the alkalinity and DIC concentrations are A_3 and $C_{DIC,3}$, respectively. The alkalinity concentration factor, χ, relates the post-selection and post-concentration alkalinity in the following way: $A_3 = \chi A_2$. In the ideal concentration case, all DIC molecules are concentrated together with the alkalinity ions, resulting in $C_{DIC,3} = \chi C_{DIC,2}$.

2.2.3. Remainder of the BE-ACS Cycle. The concentrated solution is then exposed to a vacuum, bringing the solution CO_2 partial pressure to p_{out} to collect CO_2. We use the ADICM to calculate the post-outgassing DIC concentration as a function of p_{out}: $C_{DIC,4} = C_{DIC}(A_4, p_{out})$. This relation allows us to calculate the total cycle capacity

$$C_{out} = \phi_s\left(C_{DIC,3} - \frac{A_3}{A_1}C_{DIC}(A_1, p_{out})\right) \quad (7)$$

The volume fraction parameter, ϕ_s, is needed to rescale the outgassed CO_2 relative to the fraction of the feed solution processed through the NF selection module. The stream recombination and absorption steps are not treated here but are evaluated in detail in our previous theoretical study.

3. MATERIALS AND METHODS

3.1. NF Membrane Studies. A stirred dead-end cell was used to measure the membrane properties for a range of feed solutions. The cell (HP4750) was purchased from Sterlitech Corp. and placed on a stir plate, operating at 1000 rpm. Permeation was driven by pressurized nitrogen gas, applied at a set pressure to control the permeation flow rate. Setup schematic is represented in Supporting Information Figure C2. Control experiments were conducted to ensure that stir speeds were sufficiently high to counteract the concentration polarization effect (Supporting Information Section D). Feed solution was prepared by dissolving sodium bicarbonate and sodium carbonate, purchased from Sigma-Aldrich, at known quantities into diH_2O. 100 mL of feed solution was prepared and loaded into the cell. The permeate was collected in a vessel placed on an OHAUS Scout Balance (0−2 kg range, with 0.1 g precision). Pressure was turned off and permeation stopped once 50% of solution volume, or 50 g, was collected in the permeate vessel. The permeate and concentrate solutions were then measured using a pH probe (semimicro pH electrode, 8103BN) and a combined conductivity and temperature probe (4-electrode DuraProbe, 013010MD), purchased from ThermoFisher Scientific. All experiments were conducted at 20 °C ± 2.

Each membrane was initially soaked for 1 h in diH_2O before it was loaded into the dead-end cell. Once loaded, each membrane was permeated at least three times with 100 mL feed at 40 bar with 150 mM alkalinity and 62.5% DIC-to-alkalinity ratio for pretreatment. The commercial membranes, listed in Table 1, were purchased precut to 14.6 cm^2 and systematically tested. Membrane manufacturers report that

https://doi.org/10.1021/acsestengg.4c00150
ACS EST Engg. XXXX, XXX, XXX−XXX

membranes were synthesized from different polymers, including polyamide, polypiperazine, cellulose acetate, and polysulfone (PES). All membranes are expected to be negatively charged but have different charge density, ionization pK_a values, and pore size (varying from 150 to 500 Da according to commercial specifications). To screen membranes, feed solutions with sodium cation concentrations of 50, 150, and 450 mM were prepared and tested, all at 62.5% DIC-to-alkalinity ratio (see Table 1 for membrane specifications, as well as measured bicarbonate-carbonate rejection and permeation properties). Following screening, the Filmtec NF270 membrane was selected for more detailed studies to investigate effects based on feed conditions and permeation rate.

3.2. Ion Rejection and Passage Model. To characterize the NF membranes, we evaluate the effective rejection coefficients for each species based on the following relation (derived in detail in Supporting Information Section C)

$$\Gamma_i = 1 - \frac{\ln(1 - \Phi C_{2,i}/C_{1,i})}{\ln(1 - \Phi)} \tag{8}$$

Here, $C_{1,i}$ is the feed concentration of species i in state 1, and $C_{2,i}$ is the final permeate concentration in state 2. In our experiments, the volume fraction (Φ) is 1/2. For these operating conditions, we take Γ_i to be the average rejection through the entire concentration process. In general, Γ_i can vary as a function of feed composition, pH, membrane properties, temperature, permeation rate, and other experiment conditions.

Note that the ubiquity of DIC speciation means that the rejection coefficient Γ_i for a given DIC species represents an effective rejection coefficient rather than quantifying the exact fractions of blocked and passed species i. It captures the resultant difference in concentration of a given species in the feed and the permeate after DIC speciation has acted. One effect important to understand is that RO and NF processes can either acidify or basify the permeate streams (i.e., membranes preferentially permeate more protons or hydroxides, respectively) depending on the feed conditions, thereby shifting the equilibrium between bicarbonate and carbonate ions, which would shift Γ_b and Γ_c.[34]

3.3. Ideal Cycle Energy: Multistage NF and RO Energy Model. To evaluate the work of the BE-ACS process, an ideal model for the NF and RO steps is developed. We assume the van't Hoff dilute limit approximation where the minimal osmotic pressure necessary to drive a separation process is proportional to the difference in concentration across the membrane: $\Pi = RT\sum_i(C_{1,i} - C_{2,i})$ (for reference, Supporting Information Section E considers the thermodynamic minimum work and concentration process).

First, we applied this formulation to the NF step. We assume a dual-stage process, each with its own fixed applied pressure (we note that more stages would further reduce the required work for the process but would correspond to higher process complexity, requiring more pump and membrane modules). The two stages are characterized by the initial permeated volume fraction, ϕ_1, and the final permeated volume fraction, ϕ_s, for the complete selectivity step. ϕ_s is the total volume fraction of solution passed between state 1 and state 2, so by definition, $\phi_1 < \phi_s$. The work for the first and second stage of the NF step is

$$w_{\mathrm{NF},1} = \sum_i \phi_1 RT(C_{\mathrm{c},i}(\phi_1) - C_{\mathrm{p},i}(\phi_1)) \tag{9}$$

and

$$w_{\mathrm{NF},2} = \sum_i (\phi_s - \phi_1)RT(C_{\mathrm{c},i}(\phi_s) - C_{\mathrm{p},i}(\phi_s)) \tag{10}$$

Here, the "p" and "c" subscripts indicate permeate and concentrate streams, respectively. The expression for concentration as a function of ϕ is derived in Supporting Information Section C. The volume fraction for the lowest energy for a dual stage process is given by the following relation: $\phi_1 = 1 - \sqrt{1 - \phi_s}$.[35]

Next, we assume a multistage RO process, which is made up of stages that concentrate streams by a factor of 2. The following expression, which is derived in previous work,[19] relates the work to the concentration factor χ in an ideal process with no solute loss

$$w_{\mathrm{msRO}} = RT(C_i/C_{\mathrm{out}})\log_2(\chi) \tag{11}$$

Combining the equations above and adding the work, $w_{\mathrm{vac}}(p_{\mathrm{out}})$, necessary to maintain a vacuum at a CO_2 partial pressure of p_{out}, we have a final expression for ideal cycle energy in units of kJ per mole of CO_2

$$E_{\mathrm{CO_2}} = \frac{w_{\mathrm{NF},1} + w_{\mathrm{NF},2} + w_{\mathrm{msRO}}}{C_{\mathrm{out}}} + w_{\mathrm{vac}}(p_{\mathrm{out}}) \tag{12}$$

3.4. Aqueous Dissolved Inorganic Carbon Model. We developed an ADICM based on an empirically generated aqueous chemistry model (PHREEQC Version 3). To generate DIC-to-alkalinity diagrams and computationally study ACS conditions, ADICM was used to calculate solution conditions for fixed pH, fixed partial pressure, and fixed DIC. We also used ADICM to create an inverse function that outputs the alkalinity and DIC concentrations based on the measured pH, conductivity, and temperature of a given sample. The model implements Pitzer equations to accurately calculate activity coefficients as ionic strength, temperature, and ion species are varied.[36] The model is based on activity coefficients for a wide range of ion species and their interactions and can be applied to high-salinity waters that are beyond the range of application for the Debye–Hückel theory. Based on known-sample control testing, we found that this method for measuring alkalinity and DIC concentrations yielded a <5% error for alkalinities of 150 mM and lower (see Supporting Information Section B). All solution conditions were modeled at 20 °C.

4. RESULTS AND DISCUSSION

4.1. Membrane Screen. We first screened 11 NF membranes to explore the trade-off between the bicarbonate permeation fraction and the bicarbonate-carbonate selectivity factor (Table 1). Figure 2 plots the selectivity factor and bicarbonate passage for each membrane at 50, 150, and 450 mM feed alkalinity conditions, each at a 62.5% DIC-to-alkalinity ratio. We found that there was an inverse relationship between $S_{b,c}$ and P_b: membranes with higher selectivity factors tended to have lower bicarbonate passage fractions, and lower selectivity factors corresponded to higher bicarbonate passage fractions. This is due to the fact that as the overall rejection of the membrane increased, the rejection of carbonate ions increased more strongly than the bicarbonate rejection. For all

https://doi.org/10.1021/acsestengg.4c00150
ACS EST Engg. XXXX, XXX, XXX−XXX

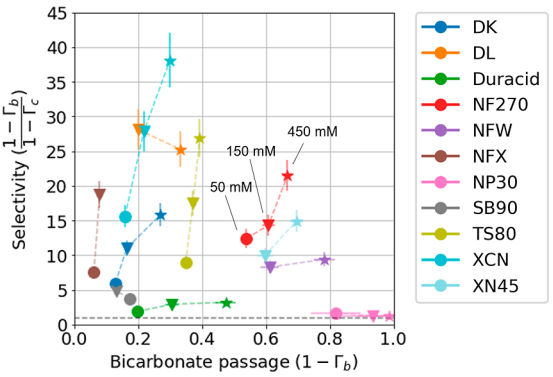

Figure 2. NF membrane screen. For each membrane, the bicarbonate-carbonate selectivity factor is plotted against the bicarbonate passage fraction. Membranes tested at 50, 150, and 450 mM feed alkalinities (Na^+), represented by a circle, triangle, and star markers, respectively. All feed conditions were prepared at 62.5% DIC-to-alkalinity ratio. Error bars represent uncertainty based on the ADICM inverse function from conductivity and pH measurements. Some membrane characterization is reported at only two feed conditions due to outlier data.

but four membranes, increasing feed alkalinity increased both the selectivity and bicarbonate passage fractions.

Because both selectivity and bicarbonate passage parameters are important for the selection module, we introduce a selection criterion to choose the best-performing membrane based on the following relation: $S_{b,c}{}^*P_b$. Maximizing this product is used as a method to select on membrane performance, though it does not uniquely identify membranes that are optimal in all operating conditions. Evaluating the selection criterion for all membranes at 150 mM alkalinity (Table 1), we find that the three best-performing membranes are Filmtec NF270 ($S_{b,c}$ = 14 and P_b = 0.61), Trisep TS80 ($S_{b,c}$ = 18 and P_b = 0.37), and Filmtec XC-N ($S_{b,c}$ = 28 and P_b = 0.22). The Filmtec XC-N membrane was identified as the most selective, reaching a selectivity factor close to 40 at the 450 mM alkalinity condition. Overall, the Filmtec NF270 membrane was selected as the best among the membranes evaluated, and more extensive studies were conducted to evaluate its properties based on varying feed conditions and permeate flux.

4.2. Characterization of Best Tested Membrane. The Filmtec NF270 membrane was studied extensively under varying feed and permeate flux conditions. Four feed alkalinity conditions—50, 150, 450, and 1000 mm—were tested. For each alkalinity condition, five DIC-to-alkalinity ratios were chosen to span carbonate-rich (high pH or low pCO_2) to bicarbonate-rich (low pH or high pCO_2) regimes: 52, 62.5, 75, 87.5, and 100%. Figure 3A reports both the carbonate and

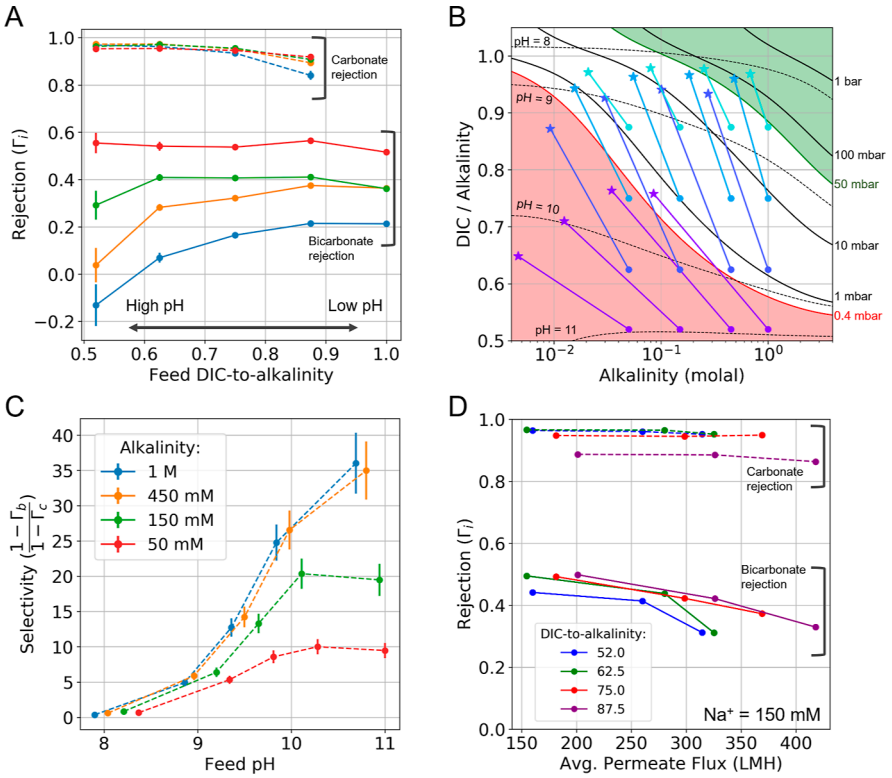

Figure 3. NF270 membrane characterization. (A) Carbonate and bicarbonate rejection factors are plotted as functions of feed DIC-to-alkalinity for four alkalinity conditions (50, 150, 450 mM, and 1 M). Negative rejection factors correspond to conditions where the concentration of the ion increases between the feed and the permeate. (B) Change in alkalinity and DIC-to-alkalinity ratio from the feed to the permeate is plotted for 20 solution conditions (circle for feed condition; star for end condition), overlaid on the diagram from Figure 1D. (C) Bicarbonate-to-carbonate selectivity is plotted against the feed pH, for each alkalinity condition. (D) Carbonate and bicarbonate rejection factors are plotted against the average permeate flux (in units of liters per meter squared per hour). Permeate flux was varied by applying 50, 60, and 70 bar of pressure (left to right for each curve). A single alkalinity condition at 150 mM was investigated at the % DIC-to-alkalinity ratios indicated. For (A–D), each point corresponds to a separate permeation run, with error bars representing uncertainty based on the ADICM inverse function from conductivity and pH measurements.

https://doi.org/10.1021/acsestengg.4c00150
ACS EST Engg. XXXX, XXX, XXX−XXX

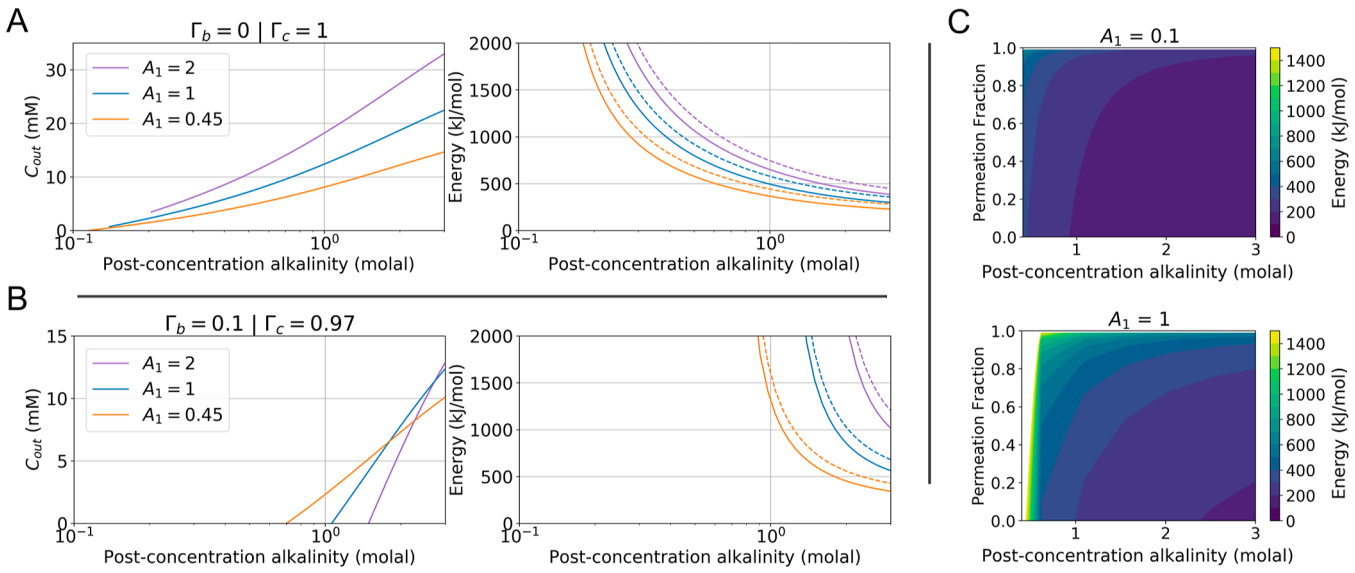

Figure 4. Process cycle capacity and energy. (A) Cycle capacity C_{out} and energy of capture as functions of post-concentration alkalinity for an ideal cycle, $\Gamma_b = 0$ and $\Gamma_c = 1$, and $\phi_s = 0.8$. Solid lines in the energy plot correspond to minimum reversible work for the NF, RO, and outgassing steps. Dashed lines correspond to the ideal multistage process. (B) Same plot as (A) but for a process based on experimental results: $\Gamma_b = 0.1$ and $\Gamma_c = 0.97$. (C) Reversible work for the NF, RO, and outgassing steps as a function of permeation fraction and post-concentration alkalinity of 0.1 (top panel) and 1 molal (bottom panel). In all cases in (A–C), $p_{in} = 0.3$ mbar and $p_{out} = 50$ mbar.

bicarbonate rejection factors as functions of the DIC-to-alkalinity ratio. Figure 3C plots the bicarbonate-carbonate selectivity factor for the same feed conditions as a function of the corresponding pH.

We find that at low pH, or equivalently high DIC-to-alkalinity ratios, the carbonate rejection factor is lower than that at high pH. For pH 9.5 and lower, the bicarbonate rejection factor is roughly flat for each feed alkalinity. In the low alkalinity regime (50 mM), the bicarbonate rejection factor is flat for all conditions. At the 1 M alkalinity and 52% DIC-to alkalinity condition, the bicarbonate rejection coefficient is negative. This could be explained by two possible effects: (1) an increased permeation driving force preferentially up-concentrating bicarbonate ions or (2) acidification of the permeate stream shifting the DIC speciation equilibrium toward bicarbonate ions.[32] For all alkalinity conditions, the carbonate rejection decreases at higher DIC-to-alkalinity ratios (or lower pH), where there is a lower relative carbonate concentration.

To understand how the membrane selectivity properties relate to the ACS process, we plot the changes in alkalinity and DIC solution composition from the feed to the permeate (Figure 3B). We overlay the partial pressure of CO_2 and pH as functions of alkalinity taken from ADICM. The feed conditions that are at high pH and high alkalinity are of greatest interest for the ACS process because those regimes allow for relatively higher absorption rate and higher cycle capacity. In these conditions, the shift from feed to permeate drops by about a pH unit and increases the partial pressure of CO_2 by about a factor of 10. The trajectories point up and to the left in the DIC-to-alkalinity diagram because the permeation process both dilutes the absolute alkalinity of the solution and increases the bicarbonate-to-alkalinity ratio.

Finally, Figure 3D plots the rejection coefficients for bicarbonate and carbonate ions as functions of average permeate flux at 150 mM alkalinity and for DIC-to-alkalinity ratios of 25, 62.5, 75, and 87.5%. Higher DIC-to-alkalinity ratios result in faster flux rates for the same applied pressure. One explanation for this effect may be due to the fact that ion permeation rates decrease as ion dehydration energies—which are higher for divalent ions than monovalent ions—increase.[37] Whereas both the carbonate and bicarbonate rejection decrease at increased permeate flux, the associated bicarbonate-carbonate selectivity factor (not-plotted) does not exhibit a flux-dependent trend. An explanation for the various observed effects is discussed in Section 4.4.

4.3. Process Assessment: Cycle Capacity and Capture Energy. The membrane characterization results we describe above directly relate to the BE-ACS cycle parameters. Although the benchtop experimental setup has significant limitations and will not match industrial-scale operating conditions, evaluating the expected cycle capacity and energy allows for benchmarking membranes and guiding future optimization efforts.

Choosing the NF270 membrane, we pick $S_{b,c} = 30$ and $P_b = 0.9$, corresponding to the experimentally achievable upper range of the characterized membrane properties (Supporting Information Figure F1). For simplicity, we apply this condition to three feed alkalinity values, 0.45, 1, and 2 molal. We do not investigate alkalinity conditions below 0.45 molal because of the decrease in selectivity factors. The 2 molal alkalinity condition was not experimentally tested with the NF270 membrane but is included in the process assessment to explore higher alkalinity ranges.

For reference, Figure 4A reports the C_{out}, or extracted CO_2, for the corresponding BE-ACS conditions, and corresponding minimum (or reversible) work (solid lines; see Supporting Information Section E for model) and ideal multistage work (dashed lines; see Section 3.3 for model) for the NF process. A range of different initial alkalinity conditions is chosen for BE-ACS cycle parameters: $p_{in} = 0.3$ mbar, $p_{out} = 50$ mbar, and $\phi_s = 0.8$. At this p_{in}, feed pH is around 10 and higher, justifying the choice of a high selectivity factor. Lower initial alkalinity conditions correspond to lower C_{out} values but also lower

https://doi.org/10.1021/acsestengg.4c00150
ACS EST Engg. XXXX, XXX, XXX–XXX

energies, reaching as low as around 250 kJ/mol for 0.45 molal conditions concentrated to 3 molal. For all conditions, higher post-concentration alkalinity both increases C_{out} and lowers the process energy.

Figure 4B plots the NF270 cycle parameters resulting from the experimentally determined parameters for NF270, $\Gamma_b = 0.1$ and $\Gamma_c = 0.97$ (Supporting Information Table F1). For the 1 mol initial alkalinity condition, a maximum C_{out} of 12.5 mM is reached, corresponding to energies slightly above 500 kJ/mol. Lower energies, below 500 kJ/mol, are possible if 0.45 molal or lower initial alkalinity conditions are chosen.

Figure 4C plots the minimum reversible work for the NF, RO, and outgassing steps at initial alkalinity values of 0.1 (top panel) and 1 molal (bottom panel), varying ϕ_s and the post-concentration alkalinity. This energy diagram shows that at all ϕ_s values, higher post-concentration alkalinity corresponds to lower energy values. Energy values decrease monotonically with the permeation fraction; however, a higher permeation fraction also increases the fraction of bicarbonate ions that are passed through the selection module, thereby increasing C_{out}. Especially at high initial alkalinity and high concentration factors, the energy begins to increase significantly above roughly $\phi_s = 0.8$, revealing a point of diminishing return.

4.4. Implications. This study demonstrates the ability of NF membrane-separation to increase the bicarbonate-to-carbonate ratio in the permeate stream or, equivalently, to increase the DIC-to-alkalinity ratio. Selectivity factors above 30, and bicarbonate passage fraction of 1 or higher, were reached under the highest-performing conditions. We found that both the feed pH and alkalinity had strong effects on the effectiveness of the cycle.

Higher feed pH corresponds to increased selectivity factors, suggesting that the ionization of charged fixed groups within the membrane, and therefore the corresponding Donnan potential, plays a dominant effect in driving selectivity.[28,38] This trend is qualitatively confirmed by simple equilibrium Donnan modeling relating bicarbonate-carbonate selectivity in the membrane to the feed pH (Supporting Information Figure G1, panel B). For negatively charged membranes, in equilibrium with alkaline feed pH, the membrane pH is shifted lower corresponding to higher bicarbonate fraction in the membrane. Equivalently, negative fixed charges on the membrane exclude carbonate ions more than bicarbonate ions and hence drive the pH lower. Past studies have characterized RO and NF membranes as negatively charged polymers with ionizable surface groups whose overall charge depends on pH. In particular, in NF270 membranes, the carboxyl groups were shown to have a second pK_a of 9.5, shifted higher relative to free solution conditions due to membrane confinement.[39] Between pH 8 and 10, NF270 membrane charge density increases from roughly 150 mM to 600 mM, as shown also in computational studies.[40] The increase in the negative charge over this pH range corresponds closely to the experimental conditions explored in this work. At pH 9, we observed a selectivity factor around 5 for all alkalinity conditions. At pH 10, we observed selectivity factors of 10, 15, 25, and 25 for alkalinity conditions of 50, 150, 450, and 1000 mM, respectively.

The bicarbonate passage and dependence of the selectivity factor on feed alkalinity, however, cannot be explained by fixed charges alone. Higher feed alkalinity conditions result in higher selectivity factors and lower bicarbonate rejection. Dielectric exclusion, electromigration, concentration polarization, and other transport effects possibly contribute to the alkalinity-selectivity dependence. Indeed, the equilibrium Donnan model detailed in the Supporting Information shows the opposite selectivity effect as a function of concentration: higher feed alkalinity conditions result in lower membrane selectivity based on the model (Supporting Information Figure G2).

One additional effect contributing to an explanation could be that the concentration drop across the membrane results in an electric field that contributes to the selectivity effect. Because the hydration radius, and the corresponding viscous drag, of bicarbonate and carbonate ions is very similar (3.64 and 3.94 Å, for bicarbonate and carbonate, respectively),[41] the charge of the ions has a dominant effect on the relative transport rates in an electric field. Therefore, in addition to the Donnan-based ion partitioning effect, the electromigration-driven flow of ions created by the concentration drop across the membrane also selects bicarbonate ions over carbonate ions.

It is possible to qualitatively evaluate this effect through the Nernst potential, which sets the voltage scale across the membrane: $V_{mem} = (RT/F)\sum_i \ln(C_{p,i}/C_{f,i})$. But without a comprehensive model, similar to ones that have been explored in past work,[42] it is not possible to quantify the magnitude of the electromigration effect on selectivity. Experiments confirm the relation between the Nernst potential and selectivity, finding that higher membrane voltage drops, at the same pH, result in higher selectivity factors (Supporting Information Figure H1). Taking an intermediate experimental condition as an example, we find that 450 mM high pH feed is diluted to roughly 40 mM. A 10× concentration drop results in approximately 60 mV across the membrane. In cases where concentration drop is very small, membrane voltages are below 10 mV. For all conditions, higher membrane voltage drops result in higher selectivity factors; at higher membrane voltages, however, selectivity exhibits a plateau, suggesting that yet another effect is needed to explain this behavior.

From the membrane screen experiments, we observe a trade-off between the bicarbonate passage and the selectivity factor. It appears that bicarbonate rejection cannot both be very low and correspond to very high selectivity factors. Higher rejection membranes result in higher selectivity factors, but they can be less effective from a process perspective due to the low bicarbonate concentration that results in the permeate. Modeling studies can help identify the physical limitation between the passage and selectivity trade-off, which is fundamental to membrane properties.[43] Process engineering innovations, such as recirculating the concentrated solution through the membrane module, can help to increase both selectivity and bicarbonate passage.

Applying the membrane characterization results to the BE-ACS cycle properties, we find that a moderate cycle capacity (10 mM) and relatively high capture energies (500 kJ/mol) can be reached with this process. The results show that, if performance is to be improved, it is important to develop NF membranes with higher bicarbonate-carbonate selectivity but comparable bicarbonate passage. Given the current membranes, process engineering can improve BE-ACS performance. For example, the feed solution can be recirculated twice or more through the NF module to exponentially improve selectivity at the cost of more energy. Permeation rate, temperature, and pressure can also be optimized to maximize the performance.

https://doi.org/10.1021/acsestengg.4c00150
ACS EST Engg. XXXX, XXX, XXX−XXX

Ideal cycle energy is found to be as low as around 250 kJ/mol for certain operating regimes, although it is expected that higher energy will be required if higher cycle capacity is desirable. For context, redox electrochemical DAC processes have been shown to reach 100 kJ/mol on bench scale systems,[16] and industrial solid sorbent and calcium-looping processes can reach energy requirements lower than 300 kJ/mol.[3] To reach similar or lower energy levels, energy recovery modules that recover energy from the salinity differences created through the NF and RO modules can significantly reduce the energy cost of capture. Modifications, such as forward osmosis modules and process stream handling, are worth exploring in future studies.[42,44]

4.4.1. Applications beyond DAC. The NF selectivity results that we report in this work are also directly applicable to approaches beyond DAC and are useful for any method that seeks to control the relative concentration of DIC species in solution. In particular, recent studies have reported that bicarbonate-rich solution can be used as a feed for electrolytic conversion to useful chemicals.[16,23,24,45] For example, Lees et al. (2020) describe a process that captures CO_2 from the atmosphere or flue gas and uses electrolyzers to convert a 3 M KHCO3 solution into CO.[46] However, the step between CO_2 absorption, which must happen at high pH conditions and therefore is dominated by carbonate ions, and the bicarbonate-rich end point is not explored. The selection and concentration steps of the BE-ACS process, implemented through NF and RO separation, provide a concrete method to convert between the contacting solution and the bicarbonate-rich state needed for electrolytic reduction.

4.5. Conclusions. This work evaluates the application of NF membrane separation to the bicarbonate-carbonate separation step of the BE-ACS. Eleven commercial membranes are screened, identifying a trade-off between effective bicarbonate passage and bicarbonate-carbonate selectivity. One membrane type, NF270, is selected as exhibiting the best characteristics and is studied extensively across a range of feed conditions and pressures. We find that the selectivity factor increases with higher feed pH, lower DIC-to-alkalinity ratios, and higher alkalinity. In the regimes we study, the highest selectivity factors exceed 30×. Applying the experimentally determined membrane properties to an ideal BE-ACS model, we characterize the cycle capacity and ideal energy. Ideal cycle energy is found to be as low as around 250 kJ/mol, and cycle capacity ranges up to 30 mM of CO_2 extracted from the feed stream. Energy recovery, for example, through the recombination of the dilute and concentrated streams using forward osmosis, and process engineering, such as introducing additional pressure stages in the RO and NF steps, are expected to significantly reduce the BE-ACS cycle energy costs.

■ ASSOCIATED CONTENT

Supporting Information

The Supporting Information is available free of charge at https://pubs.acs.org/doi/10.1021/acsestengg.4c00150.

The SI includes: Relationship between alkalinity, CO_2 partial pressure, and DIC; PHREEQC model: alkalinity and DIC inverse function; mathematical relation to determine the ion rejection coefficient from the permeate and feed concentrations; NF270 concentration polarization dead-end cell effect; thermodynamic minimum energy for DIC separation and concentration; selectivity factor and bicarbonate passage parameter maps extrapolating from the rejection data for the NF270 membrane, which is also reported in a table; equilibrium DIC Donnan model; and Nernst membrane potential across the NF membrane given experimental selectivity and concentration data (PDF)

■ AUTHOR INFORMATION

Corresponding Author

Anatoly Rinberg − *John A. Paulson School of Engineering and Applied Sciences, Harvard University, Cambridge, Massachusetts 02138, United States;* orcid.org/0000-0001-5317-087X; Email: rinberg@g.harvard.edu

Author

Michael J. Aziz − *John A. Paulson School of Engineering and Applied Sciences, Harvard University, Cambridge, Massachusetts 02138, United States;* orcid.org/0000-0001-9657-9456

Complete contact information is available at: https://pubs.acs.org/10.1021/acsestengg.4c00150

Author Contributions

CRediT: **Anatoly Rinberg** conceptualization, data curation, formal analysis, investigation, methodology, writing-original draft, writing-review & editing; **Michael J. Aziz** conceptualization, funding acquisition, methodology, project administration, supervision, writing-review & editing.

Notes

The authors declare no competing financial interest.

■ ACKNOWLEDGMENTS

This research was supported by the U.S. Department of Energy Office of Fossil Energy and Carbon Management through contract DE-FE000331964 and the Harvard Climate Change Solutions Fund. We acknowledge helpful discussions with Andrew Bergman, Tommy George, Eric Fell, and Dawei Xi, as well as Professors Matthew Suss, Oded Nir, David Keith, and Daniel P. Schrag.

■ REFERENCES

(1) *Climate, Change.: The Physical Science Basis. Contribution of Working Group I to the Sixth Assessment Report of the Intergovernmental Panel on Climate Change*; Masson-Delmotte, V., Zhai, P., Pirani, A., Connors, S. L., Péan, C., Berger, S., Caud, N., Chen, Y., Goldfarb, L., Gomis, M. I., Huang, M., Leitzell, K., Lonnoy, E., Robin Matthews, J. B., Maycock, T. K., Waterfield, T., Yelekçi, O., Yu, R., Zhou, B., Eds.; Cambridge University Press: Cambridge, United Kingdom and New York, NY, USA, 2021.

(2) Bergman, A.; Rinberg, A. The Case for Carbon Dioxide Removal: From Science to Justice. In *CDR Primer*, 2021.

(3) Pacala, S.; Al-Kaisi, M.; Barteau, M.; Belmont, E.; Benson, S.; Birdsey, R.; Boysen, D.; Riley, D.; Charles, H.; Jones, C.; Kelemen, P.; Levasseur, A.; Paustian, K.; Tang, J.; Troxler, T.; Wana, M.; Wilcox, J. *Negative Emissions Technologies and Reliable Sequestration: A Research Agenda*; The National Academies Press: Washington, DC, 2019.

(4) Lenzi, D. The ethics of negative emissions. *Glob. Sustainability* **2018**, *1*, No. e7.

(5) Anderson, K.; Peters, G. The trouble with negative emissions. *Science* **2016**, *354* (6309), 182−183.

(6) Minx, J. C.; Lamb, W. F.; Callaghan, M. W.; Fuss, S.; Hilaire, J.; Creutzig, F.; Amann, T.; Beringer, T.; de Oliveira Garcia, W.; Hartmann, J.; Khanna, T.; Lenzi, D.; Luderer, G.; Nemet, G. F.;

Rogelj, J.; Smith, P.; Vicente Vicente, J. L.; Wilcox, J.; del Mar Zamora Dominguez, M. Negative emissions—Part 1: Research landscape and synthesis. *Environ. Res. Lett.* **2018**, *13* (6), 063001.
(7) Fuss, S.; Lamb, W. F.; Callaghan, M. W.; Hilaire, J.; Creutzig, F.; Amann, T.; Beringer, T.; de Oliveira Garcia, W.; Hartmann, J.; Khanna, T.; Luderer, G.; Nemet, G. F.; Rogelj, J.; Smith, P.; Vicente, J. L. V.; Wilcox, J.; del Mar Zamora Dominguez, M.; Minx, J. C. Negative emissions—Part 2: Costs, potentials and side effects. *Environ. Res. Lett.* **2018**, *13* (6), 063002.
(8) Sanz-Pérez, E. S.; Murdock, C. R.; Didas, S. A.; Jones, C. W. Direct Capture of CO2 from Ambient Air. *Chem. Rev.* **2016**, *116* (19), 11840−11876.
(9) Keith, D. W.; Holmes, G.; St Angelo, D.; Heidel, K. A Process for Capturing CO2 from the Atmosphere. *Joule* **2018**, *2* (8), 1573−1594.
(10) Custelcean, R. Direct Air Capture of CO2 Using Solvents. *Annu. Rev. Chem. Biomol. Eng.* **2022**, *13*, 217−234.
(11) Wang, M.; Herzog, H. J.; Hatton, T. A. CO2 Capture Using Electrochemically Mediated Amine Regeneration. *Ind. Eng. Chem. Res.* **2020**, *59* (15), 7087−7096.
(12) Liu, Y.; Ye, H.-Z.; Diederichsen, K. M.; Van Voorhis, T.; Hatton, T. A. Electrochemically mediated carbon dioxide separation with quinone chemistry in salt-concentrated aqueous media. *Nat. Commun.* **2020**, *11* (1), 2278.
(13) Jin, S.; Wu, M.; Gordon, R. G.; Aziz, M. J.; Kwabi, D. G. pH swing cycle for CO2 capture electrochemically driven through proton-coupled electron transfer. *Energy Environ. Sci.* **2020**, *13* (10), 3706−3722.
(14) Seo, H.; Hatton, T. A. Electrochemical direct air capture of CO2 using neutral red as reversible redox-active material. *Nat. Commun.* **2023**, *14* (1), 313.
(15) Sodiq, A.; Abdullatif, Y.; Aissa, B.; Ostovar, A.; Nassar, N.; El-Naas, M.; Amhamed, A. A review on progress made in direct air capture of CO2. *Environ. Technol. Innovat.* **2023**, *29*, 102991.
(16) Cao, T. N.-D.; Snyder, S. W.; Lin, Yu-I.; Lin, Y. J.; Negi, S.; Pan, S.-Y. Unraveling the Potential of Electrochemical pH-Swing Processes for Carbon Dioxide Capture and Utilization. *Ind. Eng. Chem. Res.* **2023**, *62* (49), 20979−20995.
(17) Suss, M. E.; Porada, S.; Sun, X.; Biesheuvel, P. M.; Yoon, J.; Presser, V. Water desalination via capacitive deionization: what is it and what can we expect from it? *Energy Environ. Sci.* **2015**, *8* (8), 2296−2319.
(18) Elimelech, M.; Phillip, W. A. The Future of Seawater Desalination: Energy, Technology, and the Environment. *Science* **2011**, *333* (6043), 712−717.
(19) Rinberg, A.; Bergman, A. M.; Schrag, D. P.; Aziz, M. J. Alkalinity Concentration Swing for Direct Air Capture of Carbon Dioxide. *ChemSusChem* **2021**, *14* (20), 4439−4453.
(20) Rinberg, A. Concentrating Alkalinity for Direct Air Capture of Carbon Dioxide: Using Osmotic Pressure for Concentration and Separation. PhD thesis; Harvard Library, 2024.
(21) Bergman, A. M. Using Capacitive Deionization for Direct Air Capture of Carbon Dioxide: Theory and Demonstration of the Bicarbonate-Enriched Alkalinity Concentration Swing. PhD thesis; Harvard Library, 2024.
(22) Rinberg, A.; Bergman, A. M.; Aziz, M. J.; Schrag, D. P. *Experimental Demonstration of Alkalinity Concentration Swing for Direct Air Capture of CO2. Technical Report*; Harvard Univ.: Cambridge, MA (United States), 2023.
(23) Li, T.; Lees, E. W.; Goldman, M.; Salvatore, D. A.; Weekes, D. M.; Berlinguette, C. P. Electrolytic Conversion of Bicarbonate into CO in a Flow Cell. *Joule* **2019**, *3* (6), 1487−1497.
(24) Lee, J.; Liu, H.; Li, W. Bicarbonate Electroreduction to Multicarbon Products Enabled by Cu/Ag Bilayer Electrodes and Tailored Microenviroments. *ChemSusChem* **2022**, *15* (22), No. e202201329.
(25) Jones, E.; Qadir, M.; van Vliet, M. T. H.; Smakhtin, V.; Kang, S.-m. The state of desalination and brine production: A global outlook. *Sci. Total Environ.* **2019**, *657*, 1343−1356.
(26) Van der Bruggen, B.; Koninckx, A.; Vandecasteele, C. Separation of monovalent and divalent ions from aqueous solution by electrodialysis and nanofiltration. *Water Res.* **2004**, *38* (5), 1347−1353.
(27) He, R.; Dong, C.; Xu, S.; Liu, C.; Zhao, S.; He, T. Unprecedented Mg2+/Li+ separation using layer-by-layer based nanofiltration hollow fiber membranes. *Desalination* **2022**, *525*, 115492.
(28) Foo, Z. H.; Rehman, D.; Bouma, A. T.; Monsalvo, S.; Lienhard, J. H. Lithium Concentration from Salt-Lake Brine by Donnan-Enhanced Nanofiltration. *Environ. Sci. Technol.* **2023**, *57*, 6320−6330.
(29) Zhang, H.; He, Q.; Luo, J.; Wan, Y.; Darling, S. B. Sharpening Nanofiltration: Strategies for Enhanced Membrane Selectivity. *ACS Appl. Mater. Interfaces* **2020**, *12* (36), 39948−39966.
(30) Roy, Y.; Lienhard, J. H. A framework to analyze sulfate *versus* chloride selectivity in nanofiltration. *Environ. Sci.: Water Res. Technol.* **2019**, *5* (3), 585−598.
(31) Biesheuvel, P. M.; Zhang, L.; Gasquet, P.; Blankert, B.; Elimelech, M.; van der Meer, W. G. J. Ion Selectivity in Brackish Water Desalination by Reverse Osmosis: Theory, Measurements, and Implications. *Environ. Sci. Technol. Lett.* **2019**, *7*, 42−47.
(32) Gilron, J.; Gara, N.; Kedem, O. Experimental analysis of negative salt rejection in nanofiltration membranes. *J. Membr. Sci.* **2001**, *185* (2), 223−236.
(33) Fritzmann, C.; Löwenberg, J.; Wintgens, T.; Melin, T. State-of-the-art of reverse osmosis desalination. *Desalination* **2007**, *216* (1−3), 1−76.
(34) Nir, O.; Bishop, N. F.; Lahav, O.; Freger, V. Modeling pH variation in reverse osmosis. *Water Res.* **2015**, *87*, 328−335.
(35) Zhu, A.; Christofides, P. D.; Cohen, Y. Effect of Thermodynamic Restriction on Energy Cost Optimization of RO Membrane Water Desalination. *Ind. Eng. Chem. Res.* **2009**, *48* (13), 6010−6021.
(36) Parkhurst, D. L.; Appelo, C. A. J. In *Description of input and examples for PHREEQC version 3: a computer program for speciation, batch-reaction, one-dimensional transport, and inverse geochemical calculations*; *USGS Numbered Series*; U.S. Geological Survey: Reston, VA, 2013.
(37) Tang, C.; Bruening, M. L. Ion separations with membranes. *J. Polym. Sci.* **2020**, *58* (20), 2831−2856.
(38) Zhang, L.; Hamelers, H. V. M.; Biesheuvel, P. M. Modeling permeate pH in RO membranes by the extended Donnan steric partitioning pore model. *J. Membr. Sci.* **2020**, *613*, 118511.
(39) Ritt, C. L.; Werber, J. R.; Wang, M.; Yang, Z.; Zhao, Y.; Kulik, H. J.; Elimelech, M. Ionization behavior of nanoporous polyamide membranes. *Proc. Natl. Acad. Sci. U.S.A.* **2020**, *117* (48), 30191−30200.
(40) Oren, Y. S.; Biesheuvel, P. M. Theory of Ion and Water Transport in Reverse-Osmosis Membranes. *Phys. Rev. Appl.* **2018**, *9* (2), 024034.
(41) Kiss, A. M.; Myles, T. D.; Grew, K. N.; Peracchio, A. A.; Nelson, G. J.; Chiu, W. K. S. Carbonate and Bicarbonate Ion Transport in Alkaline Anion Exchange Membranes. *J. Electrochem. Soc.* **2013**, *160* (9), F994−F999.
(42) Biesheuvel, P. M.; Hamelers, H. V. M.; Suss, M. E. Theory of Water Desalination by Porous Electrodes with Immobile Chemical Charge. *Colloids Interface Sci.* **2015**, *9*, 1−5.
(43) Werber, J. R.; Deshmukh, A.; Elimelech, M. The Critical Need for Increased Selectivity, Not Increased Water Permeability, for Desalination Membranes. *Environ. Sci. Technol. Lett.* **2016**, *3* (4), 112−120.
(44) Straub, A. P.; Deshmukh, A.; Elimelech, M. Pressure-retarded osmosis for power generation from salinity gradients: is it viable? *Energy Environ. Sci.* **2016**, *9* (1), 31−48.
(45) Digdaya, I. A.; Sullivan, I.; Lin, M.; Han, L.; Cheng, W.-H.; Atwater, H. A.; Xiang, C. A direct coupled electrochemical system for capture and conversion of CO2 from oceanwater. *Nat. Commun.* **2020**, *11* (1), 4412.

https://doi.org/10.1021/acsestengg.4c00150
ACS EST Engg. XXXX, XXX, XXX−XXX

(46) Lees, E. W.; Goldman, M.; Fink, A. G.; Dvorak, D. J.; Salvatore, D. A.; Zhang, Z.; Loo, N. W. X.; Berlinguette, C. P. Electrodes Designed for Converting Bicarbonate into CO. *ACS Energy Lett.* **2020**, *5* (7), 2165−2173.

https://doi.org/10.1021/acsestengg.4c00150
ACS EST Engg. XXXX, XXX, XXX−XXX

Supplementary Information:

Bicarbonate-carbonate selectivity through nanofiltration for direct air capture of carbon dioxide

Anatoly Rinberg[†]*, **Michael J. Aziz**[†]

[†]John A. Paulson School of Engineering and Applied Sciences
Harvard University
Cambridge, Massachusetts, 02138, USA
May 2024

*rinberg@g.harvard.edu

SI pages: 11
SI figures: 8
SI tables: 1

Appendix A Dissolved Inorganic Carbon Equilibrium

A.1 Carbonate equilibrium relations

Dissolved inorganic carbon concentration (C_{DIC}), is defined as the sum of the concentration of the following three molecular species dissolved in aqueous solution:

$$C_{\text{DIC}} \equiv [\text{CO}_2]_{\text{aq}} + [\text{HCO}_3^-] + [\text{CO}_3^{-2}] \tag{A1}$$

The equilibrium balance between the species is given by the following equations:

$$H_{cp} = [\text{CO}_2(\text{aq})]/p_{CO_2} \tag{A2}$$

$$K_1 = \frac{a_{H^+} a_{HCO_3^-}}{a_{CO_2(aq)}} \tag{A3}$$

$$K_2 = \frac{a_{H^+} a_{CO_3^{-2}}}{a_{HCO_3^-}} \tag{A4}$$

Here, a_i is the activity of a given species, which relates to the concentration through the activity coefficient: $a_i = m_i \gamma_i$.

In general, the bicarbonate and carbonate equilibrium relations, K_1 and K_2, depend on temperature, ionic strength (or salinity), and the species composition of the solution, which is not evaluated in this analysis for simplicity. Throughout this study, we assume a solution at normal temperature (20°C) and pressure (1 atm) of zero salinity, $K_1 = 9.6 \times 10^{-7}\,\text{M}$ and $K_2 = 3.4 \times 10^{-10}\,\text{M}$, resulting in the first and second pK_a for the carbonate system being 6.0 and 9.5, respectively. Henry's coefficient is $H^{\text{cp}} = 0.034\,\text{M/bar}$, and the dissociation constant of water is $K_{\text{w}} = 1 \times 10^{-14}\,\text{M}^2$. We take the partial pressure of CO_2 (p_{CO_2}) to be 0.4 mbar (or 400 ppm, which is approximately atmospheric partial pressure of CO_2).

The charge-neutrality condition requires that the excess charge of conservative cations over conservative anions equal the excess charge of non-conservative anions over non-conservative cations, represented in our system in the following way:

$$A = [\text{HCO}_3^-] + 2\,[\text{CO}_3^{-2}] + [\text{OH}^-] - [\text{H}^+] \tag{A5}$$

The system of equations above can be simplified to a single equation (taking $h = [H^+]$ for simplicity), which determines the solution state for a given alkalinity and partial pressure of CO_2:

$$A = H^{\text{cp}} p_{\text{CO}_2} \left(\frac{K_1}{h} + \frac{2K_1K_2}{h^2} \right) + K_{\text{w}}/h - h \tag{A6}$$

Alternatively, the following expression determines the solution as a function of alkalinity and fixed DIC concentration:

$$A = C_{\text{DIC}} \frac{1 + 2K_2/h}{1 + h/K_1 + K_2/h} + K_{\text{w}}/h - h \tag{A7}$$

Appendix B PHREEQC model: Alkalinity and DIC inverse function

The Aqueous DIC Model (ADICM) was used to calculate the alkalinity and DIC concentration of a given solution based on pH, conductivity, and temperature measurement, and the known alkaline cation: F(conductivity, pH, temp) $\rightarrow$ A, C_{DIC}.

To test the accuracy of the inverse function, 30 test solutions with different Na^+ concentration and different known DIC fractions were prepared (Fig. B1). pH, conductivity, and temperature measurements were taken of each solution and compared to the ADICM, implementing both phreeqc.dat and pitzer.dat databases. The phreeqc.dat database found good agreement (<5%) below 150 mM alkalinity. pH agreement was high for both databases, even at intermediate and high alkalinity (>300 mM).

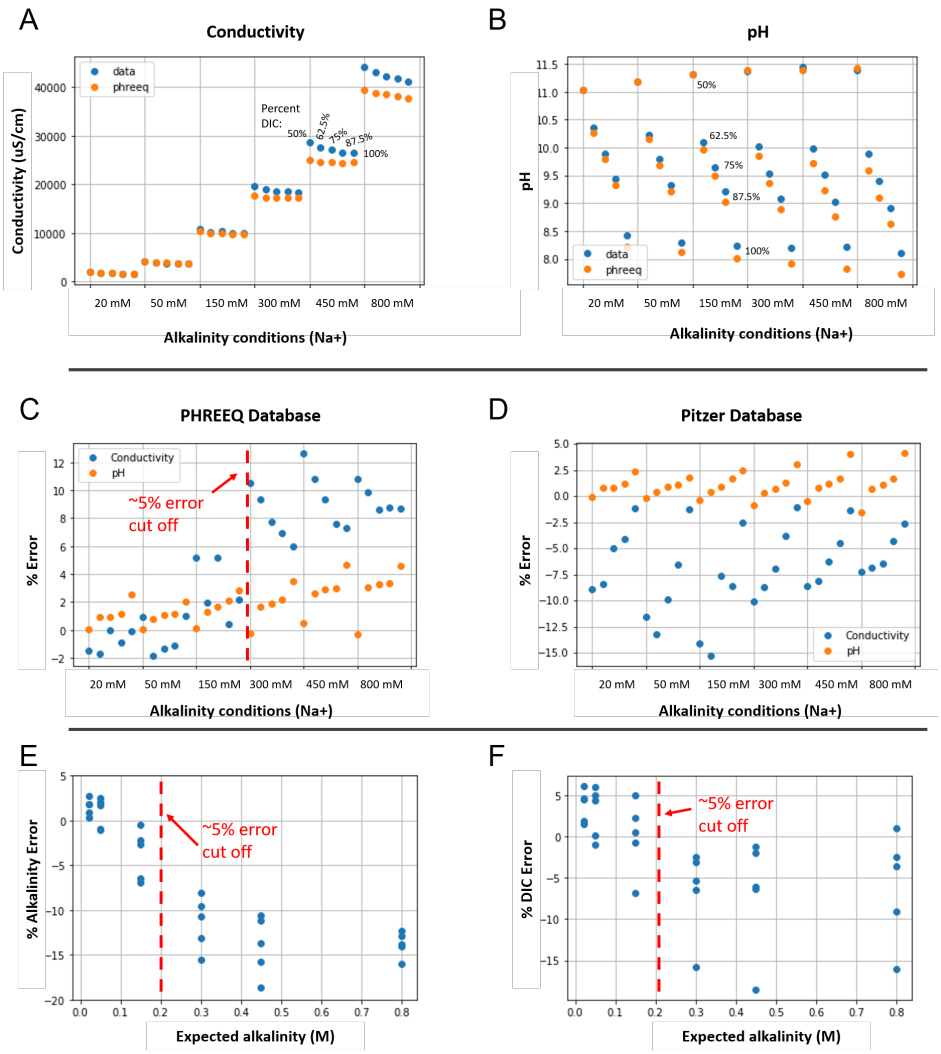

Figure B1: **ADICM error analysis.** The Aqueous DIC Model (ADICM) implementing phreeqc.dat and pitzer.dat databases was tested against 30 prepared sodium-DIC solutions.

Appendix C Dead-end cell rejection coefficient model

C.1 Concentration dependence on rejection coefficient and permeation fraction for single solute

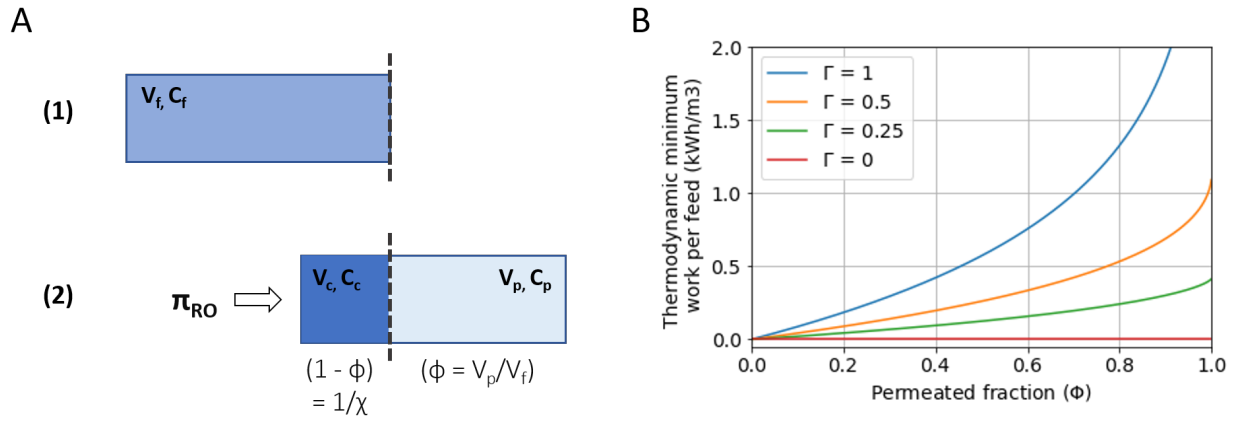

Figure C1: Osmotically-driven solution concentration and separation. (A) Single-stage reverse osmosis schematic. (B) A plot of energy per concentration of feed solution as a function of permeation fraction (ϕ) and solute rejection coefficient (Γ).

We treat a process that splits a feed solution into a concentrate and permeate streams. For simplicity we start by deriving the expression for a solution with a single solute species (Figure C1A). We find the relation between the concentrate and permeate concentrations on permeate fraction (Φ) and rejection coefficient (Γ).

Assuming, S_f, S_c, and S_p are the total amount of solute (in units of moles) in the feed, concentrate, and permeate, respectively, we write down the following mass conservation relation:

$$S_f = S_c(\Phi) + S_p(\Phi) \tag{C1}$$

The concentrate and permeate stream conditions are a function of the permeation fraction, which is defined as the ratio of permeated volume to feed volume: $\Phi = V_p/V_f$. We can then convert solute amount to concentration: $C_c(t) = S_c(t)/V_c(t)$ and $C_p(t) = (S_f - S_c(t))/V_p(t)$.

Defining Γ as the solute rejection coefficient, or the fraction of solute blocked by the membrane, allows us to write down the following differential relationship:

$$dS_c = \Gamma C_c(\Phi) dV_c \tag{C2}$$

Plugging in from above and with $dV_c = -V_f d\Phi$:

$$dS_c = -\Gamma \frac{S_c(t)}{V_c(t)} V_f d\Phi \tag{C3}$$

Finally, taking $V_f/V_c = 1/(1-\Phi)$, we integrate both sides:

$$\int \frac{dS_c}{S_c(\Phi)} = -\Gamma \int \frac{d\Phi}{(1-\Phi)} \tag{C4}$$

$$ln(S_c(t)) = -\Gamma ln(1 - \Phi(t)) + const. \tag{C5}$$

The initial condition $C_c(0) = C_f$ gives the final expressions for concentrate and permeate concentrations:

$$C_c(\Phi) = \frac{C_f}{(1-\Phi)^{\Gamma}} \tag{C6}$$

$$C_p(\Phi) = C_f \frac{1-(1-\Phi)^{1-\Gamma}}{\Phi} \tag{C7}$$

In the limit where $\Gamma \longrightarrow 1$, the permeate concentration goes to 0, and the concentrate can be written in terms of the concentration factor ($\chi = 1/(1-\Phi)$):

$$C_c(\Phi) = \chi C_f \tag{C8}$$

C.2 Multiple ion species generalization

In general, a solution will contain multiple ion species, each with different rejection coefficients. We extend the derivation from the previous section to apply to multiple species by assuming that each species is linearly independent, but that all species share the permeation fraction as a common state variable. The index, i, denotes the ion species in solution. In the simplest case, the species are the alkalinity carrier (K^+ or Na^+), bicarbonate, carbonate, and hydroxide ions.

$$C_{c,i}(\Phi) = \frac{C_{f,i}}{(1-\Phi)^{\Gamma_i}} \tag{C9}$$

$$C_{p,i}(\Phi) = C_{f,i} \frac{1-(1-\Phi)^{1-\Gamma_i}}{\Phi} \tag{C10}$$

Rewriting in terms of Γ, we have:

$$\Gamma_i = 1 - \frac{ln(1-\Phi C_{p,i}/C_{f,i})}{ln(1-\Phi)} \tag{C11}$$

C.3 Dead-end cell experimental method

Figure C2 plots the dead-end cell method for characterizing membrane properties as a function of initialized feed solution.

Appendix D NF270 Concentration Polarization Dead-end Cell Effect

The concentration polarization effect is evaluated in the dead-end cell by systematically varying the stir bar rotation rate for alkalinity of 150 and 450 mM (Fig. D1. For the 150 mM solution, the permeation rate is independent of stir rate above rpm of 700. For 450 mM solution, permeation rate is independent of stir rate at least at 1400 rpm and higher.

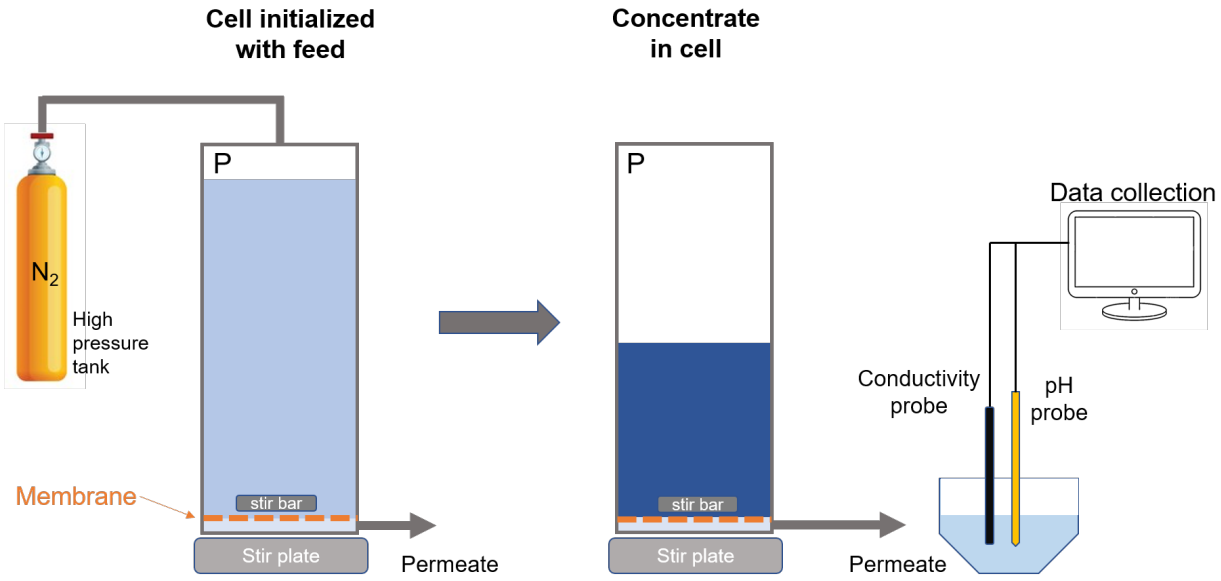

Figure C2: **Dead-end cell membrane characterization method.**

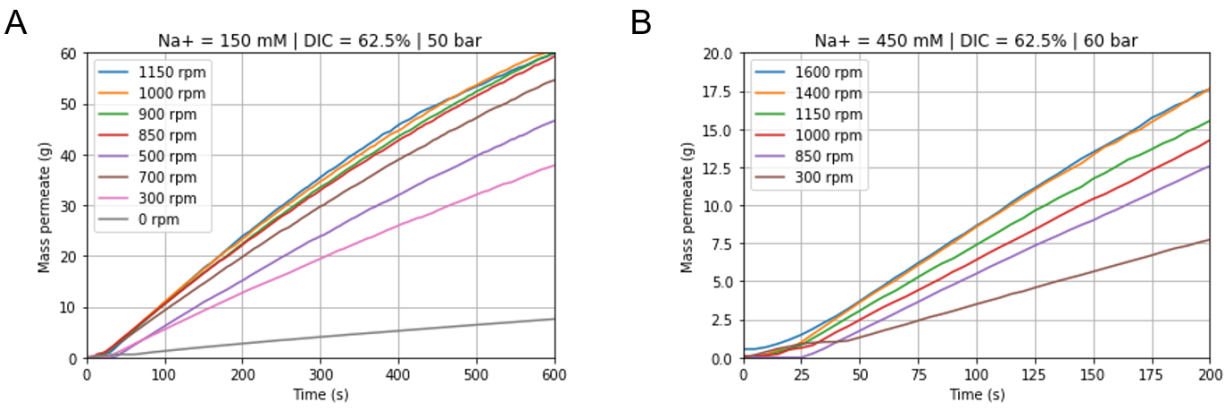

Figure D1: NF270 dead-end cell permeation rate at different stir rates.

Appendix E Thermodynamic minimum energy for DIC separation and concentration

Calculating the minimum thermodynamic amount of energy required to separate aqueous DIC solutions allows us to understand how effectively energy inputs are being used by this process. The theoretical minimum energy, which is independent of the s method chosen, is realized when the separation occurs as a reversible thermodynamic process. The energy for the separation will be equal in magnitude but opposite in sign to the free energy of mixing. To calculate the thermodynamic minimum energy, we rely on the van't Hoff approximation at dilute conditions, which can be derived mathematically as follows:

$$\Delta G_{mix} = -T\Delta S_{mix} = RTln(\gamma_w x_w) \tag{E1}$$

Here, ΔG_{mix} is the Gibbs free energy of mixing solutes into water, which results in a water activity coefficient of γ_w and molar fraction of x_w. R is the gas constant and T is the temperature in Kelvin. Because DIC species can

convert into one another, we do not differentiate their mole fraction, and we do not consider the additional entropy of mixing different ion species.

Gibbs free energy considers non-volume expansion work (applicable here due to the incompressibility of water), which allows us to introduce a volume variable, V, and define an osmotic pressure (Π) as:

$$\Pi = -(RT/V)ln(\gamma_w x_w) \tag{E2}$$

In ideal solution conditions, we can assume $\gamma_w = 1$, convert the molar fraction of the solvent to the solute, $x_w = 1 - x_s$, and make the following approximation through the Taylor series expansion: $ln(1 - x_s) \approx -x_s$. Combining the above relations, we can write:

$$\Pi = CRT \tag{E3}$$

Here C is the molar concentration in moles per liter. This simplified formulation can be extended to the osmotic pressure between two solutions with different solute concentrations:

$$\Pi = RT(C_1 - C_2) \tag{E4}$$

Writing the concentrations of species i as $C_{1,i}$ and $C_{2,i}$ allows us to define the differential work per volume as:

$$dw = \Pi d\phi = \sum_i RT(C_{1,i}(\phi) - C_{2,i}(\phi))d\phi \tag{E5}$$

Note that while it is important to differentiate bicarbonate and carbonate ions for the purposes of partial pressure and C_{out} analysis, from an energetic perspective, we treat bicarbonate, carbonate, and aqueous CO_2 as indistinguishable.

In the bicarbonate-carbonate selective ACS cycle, feed solution is first separate into a bicarbonate-rich and bicarbonate-depleted stream (Step $2 \rightarrow 3$), and then the bicarbonate-rich stream is concentrated (Step $3 \rightarrow 4$). Splitting up the work in this way allows us to write:

$$w_{1\rightarrow 3} = w_{min,sel} + w_{min,conc} \tag{E6}$$

The thermodynamic minimum work necessary for the selectivity step is then given by integrating over the permeation fraction from 0 to the final permeation fraction (ϕ):

$$w_{min,sel} = RT \sum_i \int_0^{\phi} \Big(C_{1,i}(\phi') - C_{2,i}(\phi')\Big)d\phi' \tag{E7}$$

$C_{1,i}(\phi)$ and $C_{2,i}(\phi)$ are the concentrations of solute i as a function of ϕ through the selectivity step, satisfying the following mass conservation relation: $C_{1,i}(0) = C_{1,i}(\phi)(1 - \phi) + C_{2,i}(\phi)\phi$.

The concentration step is characterized by ideal separation of water, and a concentration factor for Step $3 \rightarrow 4$, χ, which simplifies the energy derivation to:

$$w_{min,conc} = RT\Big(\sum_i C_{2,i}(\phi)\Big)ln(\chi) \tag{E8}$$

Finally, to relate the thermodynamic minimum work to a CO_2 capture energy, we divide the work by C_{out}, which is the CO_2 collected from solution and is a function of process conditions determined by aqueous carbonate chemistry relations. This gives:

$$E_{min,\mathrm{CO_2}} = \frac{w_{min,sel} + w_{min,conc}}{C_{out}} + w_{vac}(p_{out}) \tag{E9}$$

Here, $w_{vac}(p_{out})$ is the vacuum work for a given outgassing partial pressure.

Appendix F BE-ACS NF270 Membrane Parameter Map

Experimental data from the NF270 bicarbonate-carbonate selectivity experiments allows for evaluating the selectivity factor ($S_{b,c}$) and the bicarbonate passage factor (P_b) as functions of feed solution conditions. Figure F1 plots these two experimentally determined variables over a DIC-to-alkalinity and alkalinity parameter space. Full dataset is reported in Table F1.

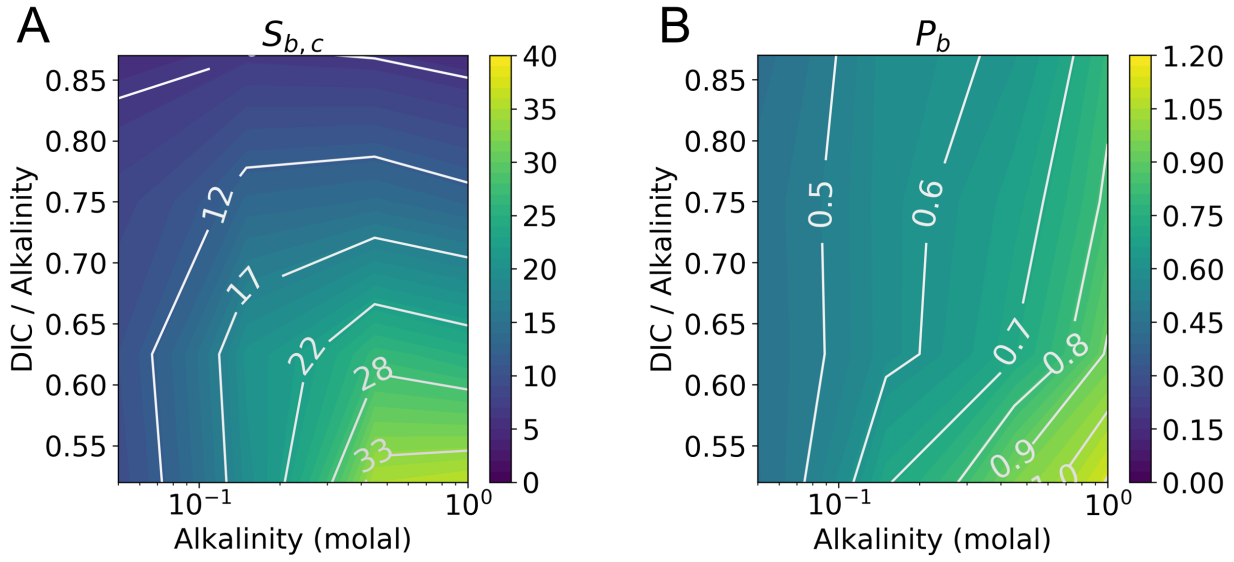

Figure F1: **Experimental parameter map.** The selectivity factor ($S_{b,c}$; panel A) and the bicarbonate passage factor (P_b; panel B) are plotted as functions of feed DIC-to-alkalinity and alkalinity. Data based on Table F1

Table F1: NF270 selectivity and rejection data.

Feed conditions				Permeate conditions			Selectivity & rejection		
Alkalinity (molal)	DIC/A	pH	Cond (mS/cm)	pH	Cond. (mS/cm)	Permeation (LMH)	$S_{b,c}$	Γ_b	Γ_c
1.0	1.00	7.90	46.8	8.14	38.3	149.4	-	0.213 ± 0.009	-
1.0	0.88	8.86	46.2	8.27	32.7	121.3	4.9	0.214 ± 0.010	0.840 ± 0.019
1.0	0.75	9.36	48.2	8.42	25.2	93.4	12.7	0.165 ± 0.012	0.934 ± 0.007
1.0	0.62	9.84	46.4	8.73	16.1	73.6	24.8	0.069 ± 0.021	0.962 ± 0.004
1.0	0.52	10.69	47.0	9.73	5.8	60.1	36.0	-0.131 ± 0.088	0.969 ± 0.002
0.45	1.00	8.04	24.8	8.21	18.7	251.1	-	0.364 ± 0.005	-
0.45	0.88	8.96	23.1	8.35	15.1	225.4	5.9	0.375 ± 0.006	0.894 ± 0.013
0.45	0.75	9.50	25.2	8.51	11.5	178.9	14.2	0.322 ± 0.008	0.952 ± 0.005
0.45	0.62	9.98	25.8	8.83	6.9	157.3	26.5	0.282 ± 0.014	0.973 ± 0.003
0.45	0.52	10.80	25.9	9.81	2.7	137.3	35.0	0.038 ± 0.073	0.973 ± 0.002
0.15	1.00	8.21	9.7	8.26	7.2	378.2	-	0.361 ± 0.004	-
0.15	0.88	9.20	9.8	8.50	5.6	326.2	6.4	0.410 ± 0.006	0.908 ± 0.011
0.15	0.75	9.65	10.5	8.72	4.0	298.5	13.3	0.406 ± 0.008	0.955 ± 0.005
0.15	0.62	10.11	10.3	9.11	2.3	280.2	20.4	0.409 ± 0.015	0.971 ± 0.003
0.15	0.52	10.94	10.8	10.10	1.1	260.1	19.5	0.292 ± 0.061	0.964 ± 0.001
0.05	1.00	8.37	3.6	8.48	2.2	334.1	-	0.516 ± 0.003	-
0.05	0.87	9.34	3.7	8.75	1.7	307.5	5.3	0.564 ± 0.005	0.918 ± 0.010
0.05	0.75	9.81	3.8	9.06	1.3	293.5	8.6	0.537 ± 0.009	0.946 ± 0.006
0.05	0.62	10.28	4.0	9.52	0.8	283.4	10.0	0.541 ± 0.019	0.954 ± 0.004
0.05	0.52	11.00	4.3	10.33	0.5	277.1	9.5	0.554 ± 0.043	0.953 ± 0.001

Appendix G Equilibrium DIC Donnan model

Donnan membrane potential arises from the inability of certain ions to diffuse out of one phase and into another. Donnan equilibrium theory has been used to model effects in ion-exchange, NF, and RO membranes, among other systems.[28]

The following is a system of equations modelling a DIC solution interacting with a membrane of charge X. Here, C_i denotes the concentration of a given species, with the variable A meaning alkalinity (i.e., either K^+ or Na^+ ions); and b and c representing the concentration of HCO_3^- and CO_3^{-2} ions, respectively. Two compartments are assumed: inside the membrane, denoted by the "m" subscript, and the solution itself, denoted by the "s" subscript. A more realistic model involves reactions between aqueous CO_2, bicarbonate, and carbonate species, as well as treatment of water disassociation. The relevant chemical equilibrium relations for the DIC system can be written in the following way:

$$K_1 = \frac{C_h C_b}{C_a} \tag{G1}$$

$$K_2 = \frac{C_h C_c}{C_b} \tag{G2}$$

And the water equilibrium relation is:

$$K_w = C_h C_{oh} \tag{G3}$$

More accurately, the activity of each species, a_i, should be accounted for in the equilibrium relation, relating to the concentration through the activity coefficient in the following way: $a_i = C_i \gamma_i$. However, for the sake of this work, and because the activity coefficients within membranes and electrodes are poorly understood, we evaluate the simpler model with concentrations only.

Finally, the charge-neutrality condition must be introduced, including proton and hydroxide ions. As before, the membrane charge neutrality condition requires an additional variable, X, which defines membrane charge, resulting in:

$$0 = X + C_{A,m} - C_{b,m} - 2C_{c,m} - C_{oh,m} + C_{h,m} \tag{G4}$$

Given that the system of equations between the DIC species, and separately between protons and hydroxides, it is sufficient to write a Donnan relation for only one species from each family of reactions:

$$C_{A,m} = C_{A,s} \Phi_A e^{-(+1)\Delta\phi_D} \tag{G5}$$

$$C_{b,m} = C_{b,s} \Phi_b e^{-(-1)\Delta\phi_D} \tag{G6}$$

$$C_{c,h} = C_{h,s} \Phi_h e^{-(+1)\Delta\phi_D} \tag{G7}$$

This gives a system of equation with 7 unknowns and 6 equations (as the $K1$ equation is only necessary for calculating the aqueous CO_2 concentration). The feed solution condition is assumed as given, as it is directly measurable.

A final equation combining the Donnan terms and the equilibrium relations can be written down as follows:

$$0 = X + C_{A,s}\Phi_A e^{-\Delta\phi_D} - C_{b,s}\Phi_b e^{\Delta\phi_D}\left(1 - \frac{2K_2}{C_{h,s}\Phi_h e^{-\Delta\phi_D}}\right) - \frac{K_w}{C_{h,s}\Phi_h e^{-\Delta\phi_D}} + C_{h,s}\Phi_c e^{-\Delta\phi_D} \tag{G8}$$

In the equation above, all but the $\Delta\phi_D$ is know, and the equation can therefore be solved for the Donnan potential of the system. Once the Donnan potential is known, all other terms within the membrane are uniquely defined.

We note that the choice of which DIC species to use for the Donnan relation is arbitrary. Choosing bicarbonate or carbonate is equivalent and results in the same functional form, as the Boltzmann term is propagated through the K_2 equilibrium relation.

We can further add an important complexity, accounting for the pH-dependent ionization of chemical groups inside the membrane. In general, this modifcation will take the following functional form when one chemical group (e.g. COOH) is present:

$$X = \frac{X_0}{1 + C_{h,m}/K_x} \tag{G9}$$

The equations above reveal that the bicarbonate and carbonate species will be affected differently by the Donnan potential through their valence charge, and suggests one effect that will drive ion selectivity. However, the shift in pH within the membrane or electrode will also result in speciation between bicarbonate and carbonate ions. Figures

G1 and G2 plot the membrane concentrations, as well as the bicarbonate-carbonate selectivity within the membrane as functions of feed concentration and pH.

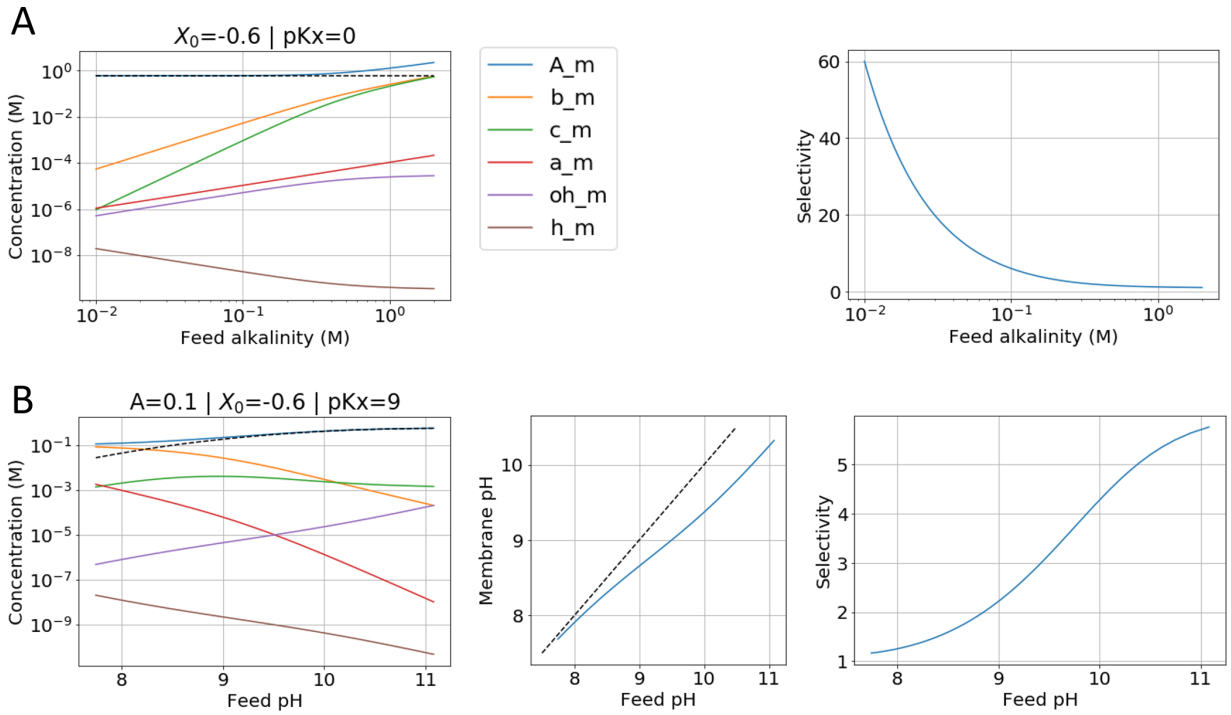

Figure G1: **Equilibrium Donnan model.** (A) Equilibrium Donnan model plotting the alkalinity, bicarbonate, carbonate, aqueous CO_2, hydroxide, and proton concentrations as functions of feed alkalinity. Right panel plots the bicarbonate-carbonate selectivity within the membrane as a function of alkalinity. Charged groups are assumed to be pH-independent and fixed at -0.6M. (B) The same output plotted as a function of feed pH, with fixed charge ionization turned on based on $pK_x = 9$. Middle panel plots the membrane pH as a function of feed pH. Dashed line has a slope of unity.

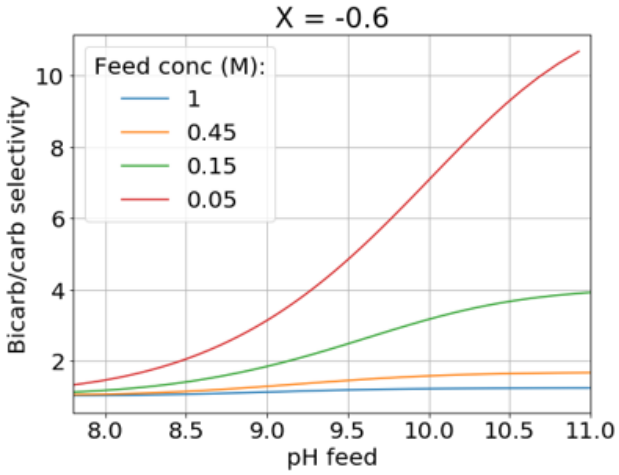

Figure G2: **Donnan model concentration effect.** Equilibrium Donnan model plotting the bicarbonate-carbonate selectivity within the membrane as a function of feed pH. Different curves correspond to different feed alkalinity conditions from 0.05 to 1 M. Fixed charge is negative at $X_0 = -0.6$ M, with ionization constant of $pK_x = 9$.

Appendix H Nernst membrane potential.

To evaluate the effect of electromigration on selectivity, the Nernst membrane potential can be calculated for each NF experiment:

$$V_{mem} = \frac{RT}{zF} ln(C_p/C_f) \tag{H1}$$

The alkalinity drop between the permeate and the feed throughout the dead-end experiment runs sets the permeate and feed concentration ratio, allowing for setting set z=1. However because the feed concentration increases in dead-end experiments, it suffices to use the alkalinity rejection coefficient, Γ_A, to evaluate the overall membrane potential drop:

$$V_{mem} = \frac{RT}{F} ln(1 - \Gamma_A) \tag{H2}$$

Figure H1 plots the selectivity factor as a function of the membrane potential based on the above relation for all experimental conditions.

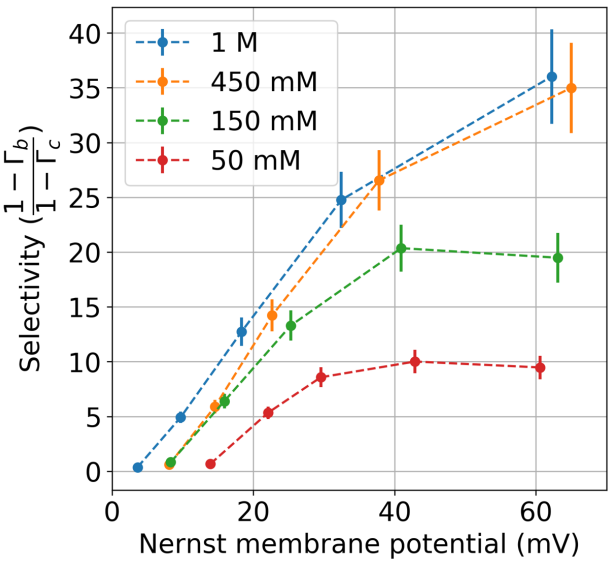

Figure H1: **NF experiments Nernst membrane potential.** Bicarbonate-carbonate selectivity is plotted as a function of Nernst membrane potential in mV based on the alkalinity rejection for different experimental conditions.